

DIRECT PRINTING OF FINE COPPER LINES BY SELF-ORGANIZED CONVECTIVE FLOW

T. CUK¹, S.M. TROIAN², C.M. HONG¹ and S. WAGNER¹

¹Dept. of Electrical Engineering and ²Dept. of Chemical Engineering,
Princeton University, Princeton, N. J. 08544-5263

ABSTRACT

We have developed a technique for the printing of fine copper lines using solutions of a metal organic precursor, copper hexanoate (CuHex). Liquid ribbons 500 μm wide, deposited on a glass substrate either by ink-jetting or capillary writing, are observed to split into two or four finer lines depending on the solution concentration. Surface profiles indicate that the thickness, width and number of lines formed are strongly dependent on the solution viscosity and volume per unit length deposited. From particle tracking analysis and surface profiling, we find that a combination of two key effects - contact line pinning and evaporative cooling - accrete solute along two boundaries of the flow. The pinning produces an exterior line pair; the evaporative cooling induces Bénard convection cells which accrete material into an interior line pair. These accretion patterns are then annealed to form pure copper lines.

INTRODUCTION

Several recent studies have explored the phenomenon leading to self-organized ring formation in drying drops [1-5]. This formation is sometimes called the “coffee-stain effect” since a dried coffee droplet develops a darkened ring stain at the edge. There is interest in controlling this solute deposition for applications like high resolution printing, nanoparticle arrays for light emitting and processing devices, colloidal self-organization for photonic crystals and the direct printing of copper interconnects. In this paper, we demonstrate the use of this process for the direct printing of fine copper lines. Past studies have targeted pinning of the contact line (i.e. the junction at the air-liquid-solid interface) as the source of solute accretion in dried droplets. Both chemical inhomogeneities or roughness caused by surface effects or particle agglomeration can pin an advancing or receding contact line [6,7]. This pinning leads to solute accretion either by capillary flow from the droplet apex to edge [1,2] or meniscus pinning by particle accretion [5]. We have studied the evaporation of long liquid ribbons which create one or two pairs of parallel solute lines by a combination of contact line pinning and thermocapillary convection due to Bénard-Marangoni flow.

EXPERIMENT

Liquid ribbons of copper hexanoate, $\text{Cu}_2(\text{OH})_2(\text{O}_2\text{CR})_4$ with $\text{R} = (\text{CH}_2)_4\text{CH}_3$, dissolved in chloroform (CHCl_3) by heating to 63°C , were directly written onto cleaned glass slides with fine glass capillaries (100 μm ID). After drying, this solution was reduced to pure copper metal by annealing [8]. As the solvent evaporated, the CuHex was observed to accrete into pairs of parallel lines narrower in width than the original liquid ribbon. Figure 1 shows an example of

a single pair of pure copper lines formed at the original site of the parallel contact lines. The same phenomenon has been obtained by ink-jetting a solution of CuHex in isopropanol [8]. We studied the drying behavior of three (initial) concentrations: $C = 0.02, 0.06, 0.10$ g/ml CuHex/CHCl₃. The associated solution properties, as well as the inferred volume/length deposited, effective contact angle, and width of the dried liquid ribbon, are given in Table 1. A Dektak profilometer was used to obtain scans of the dried solid lines in cross-section as shown in Fig. 2. The more viscous solutions flowed more slowly from the glass capillary dispensing less liquid volume per unit length. The volume/length was inferred from the ratio $\rho A_{\text{CuHex}}/C$ where $\rho=1.1$ g/ml is the density of copper hexanoate, A_{CuHex} is the cross-sectional area of the entire dried ribbon as measured by the profilometer, and C the initial solution concentration.

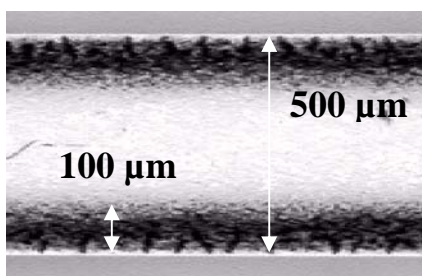


Figure 1 Optical micrograph of a pair of copper lines 100 μm wide formed by writing a 544 μm wide liquid ribbon of 0.10 g CuHex/ ml CHCl₃ on a glass slide.

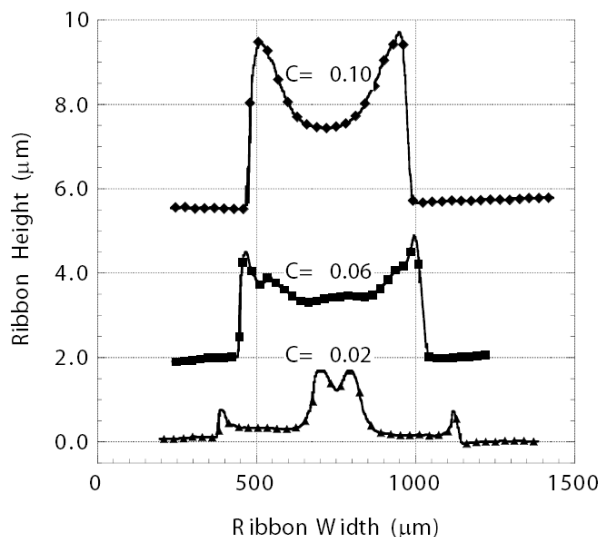


Figure 2 Thickness profiles of dried stripe patterns formed from precursor liquid solutions with $C = 0.02, 0.06,$ and 0.10 g/ml CuHex/CHCl₃.

Expt.	Concentration ($C = \text{g/ml}$)	Viscosity ($\mu = 10^{-4}$ Pa-s)	Vol/Length (10^{-5} ml/cm)	Contact angle θ°	Dried ribbon width (μm)
control	0.000	5.37	---	8.0	---
1a	0.100	30.65	15.5	17.8	544
1b	0.060	10.67	16.7	15.5	605
1c	0.021	6.56	22.3	12.5	780
2a	0.102	30.65	3.78	6.9	434
2b	0.063	10.67	6.27	4.0	741
2c	0.021	6.56	8.70	3.3	955
3a	0.062	10.7	3.90	7.0	436
3b	0.062	10.7	48.0	14.4	1070

Table 1 Parameter values for the direct writing of copper lines by the capillary method. Profiles corresponding to entries 1a-1c are shown in Fig. 1.

The initial contact angle was estimated from the value of the volume per unit length deposited assuming the liquid ribbon formed a segment of a cylinder in cross-section. The lower viscosity solutions produced a lower contact angle, as expected. As shown in Fig. 2, the least concentrated (and therefore least viscous) solution produced two lines pairs – a shallow pair at the original contact line and a thicker pair about the center. The highest concentration solution produced only two thick line pairs at the contact line. In general, our studies show that the lower viscosity solutions always produce two symmetric line pairs, one pair localized to the original contact lines and a second pair localized about the ribbon center. A second study, designated as Expt. 2a-c in Table 1, yielded essentially the same profile trends as shown in Fig. 2. We also conducted one study in which the concentration was held fixed at $C=0.062$ g/ml but the volume/length dispensed varied between $3.9 - 48.0 \cdot 10^{-5}$ ml/cm (see entries 3a-b in Table 1). The deposition with the larger volume/length dispensed allowed the formation of two line pairs as shown in Fig. 3. These runs indicate that the deposition of a liquid ribbon with larger area in cross-section, whether by dispensing the solution from a wider capillary or by decreasing the solution viscosity, produces multiple line pairs.

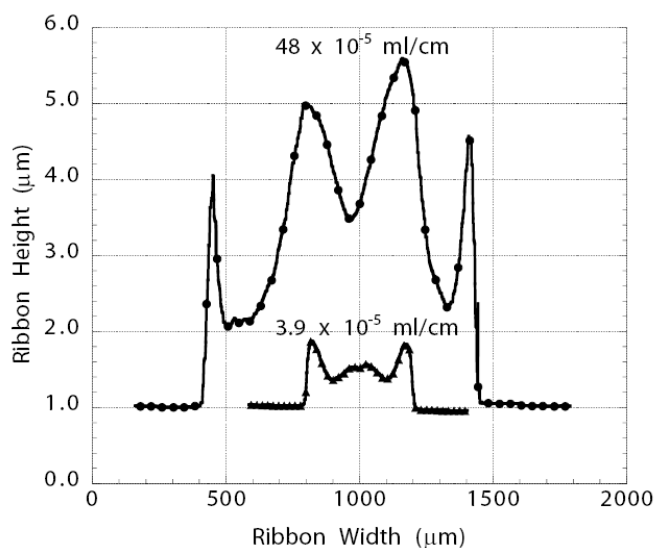


Figure 3 Surface profiles of dried liquid ribbons with dispensed volume/length = 3.9×10^{-5} and 48×10^{-5} ml/cm. The two ribbons were written with different sized capillaries.

The mechanisms in the literature [1-5] describing material accretion due to contact line pinning cannot explain the formation of the interior line pairs we have observed. Occasionally, if a liquid depins while drying, multiple line formation is possible, but each line formed corresponds to the location of the contact line as it undergoes stick-slip motion [5]. In order to determine whether the interior line pairs were either formed by successive depinning or rather by surface flows established by thermocapillary convection, we conducted flow visualization studies in which we seeded low viscosity solutions with $2 \mu\text{m}$ silica beads and imaged the bead trajectories during evaporation. Video microscopy was used to track the trajectories of the silica beads in pure chloroform (as a control experiment) and in low concentration solutions of CuHex in chloroform ($C = 0.002$ g/ml). Flow visualization did not work well at the higher concentrations listed in Table 1 because the solutions were too dense and opaque. However, we found that the location of the external line pair in the more

concentrated solutions corresponded well to the location of the CuHex and silica beads in the low concentration experiments. These low concentration studies allowed us to visualize the flow patterns and particle accretion at the contact line and throughout the surface of drying droplets or liquid ribbons. Since the liquid ribbons produced by our glass capillaries were rather thin, the evaporation was extremely rapid. Many of the experiments performed were therefore conducted with larger sized droplets but the different convection patterns observed, as well as their time of formation and location, were the same for all practical purposes in either geometry.

RESULTS

The flow patterns observed were extremely similar to those first described in the work by Zhang, Wang and Duh [9-11] in their study of evaporation-induced convection in pure solvent droplets. For highly volatile liquids, the evaporation process establishes a temperature differential between the air-liquid surface and the solid substrate. The latent heat of evaporation produces a significant overall cooling of the free surface; however, because of the non-uniform height of the droplet, there also develops a tangential variation in temperature. In very thin liquid films, the thermal variation produces differences in the local surface tension which give rise to Bénard-Marangoni convection rolls or hexagonal cells. These result from a well known hydrodynamic instability. In Fig. 4 we sketch the different regimes observed in cross-section in an evaporating liquid ribbon prone to forming two pairs of accretion lines.

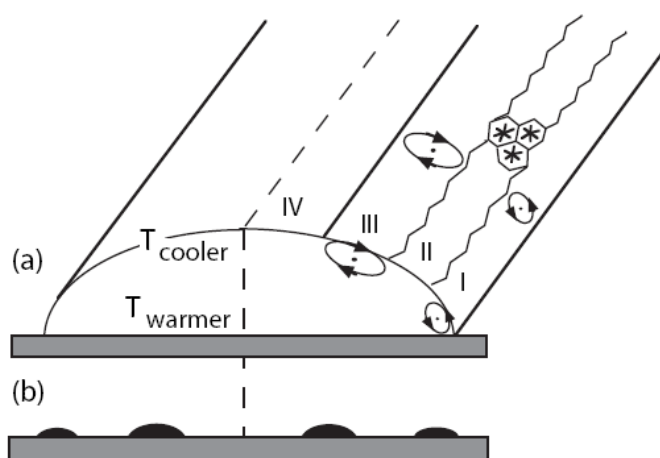


Figure 4 Schematic diagram (not drawn to scale) of flow patterns observed in an evaporating solution of CuHex, along with accretion zones. (a) Regions I and III develop oppositely directed Bénard rolls, region II undergoes formation of polygonal and hexagonal Bénard convective cells, and region IV presents a stagnant cap with no perceptible surface motion.

(b) Typical accretion patterns observed for low viscosity ($C=0.002$ g/ml) CuHex solutions.

Duh and Wang [11] conducted numerical studies which showed that convective rolls can be established by either buoyancy (Rayleigh instability) or surface tension gradient forces (Bénard instability). For a liquid ribbon with cylindrical cap cross-section, the Rayleigh number, which describes the competition between buoyancy driven convection, viscous shear and thermal diffusion, is defined as $Ra = (\beta g \Delta T R^3) / \nu \alpha$, where β is the thermal expansion coefficient, g is the gravitational constant, ΔT is the maximum temperature variation between the air-liquid and liquid-solid surface, R is the initial cylinder base radius, ν is the kinematic viscosity and α is the thermal diffusivity. The Marangoni number, which describes the competition between shear driven flow caused by surface tension gradients, viscous shear and thermal diffusion, is

defined as $Ma = (R \partial\sigma/\partial T \Delta T) / \mu \alpha$, where σ and μ denote the liquid surface tension and viscosity, respectively. In our studies, the ratio Ma/Ra exceeds 10^{+6} , a clear indication that the flow is completely dominated by Marangoni (surface tension gradient) stresses.

According to the theory of Bénard instabilities, once the critical Ma number is exceeded, a liquid film can either form rolls or hexagonal cells depending on the details of the boundary conditions. Although the number for criticality has not been determined for a droplet undergoing evaporation, experimentally we find that oppositely directed convective rolls develop in regions I and III while polygonal and hexagonal cells form in region II. Interestingly, region IV remains stagnant even while neighboring regions undergo strong surface flows. This may be due to the fact that the thermal gradient near the drop apex is insufficient to drive this region unstable but further studies need to be conducted to determine if this is the cause. As the liquid film dries, regions II and III are observed to migrate towards the stationary cap eventually depositing much of the solute originally contained in this sections along the periphery of region IV. The formation of the interior line pair is directly correlated to the presence of this inward migration and final accretion of solute. Figure 5 depicts two snapshots of this solute migration from region III to IV in a droplet of chloroform seeded with silica beads for visualization. Measurements of the final location of the dried solute stripes correspond well with the initial position of the contact line and the periphery of the stagnant cap.

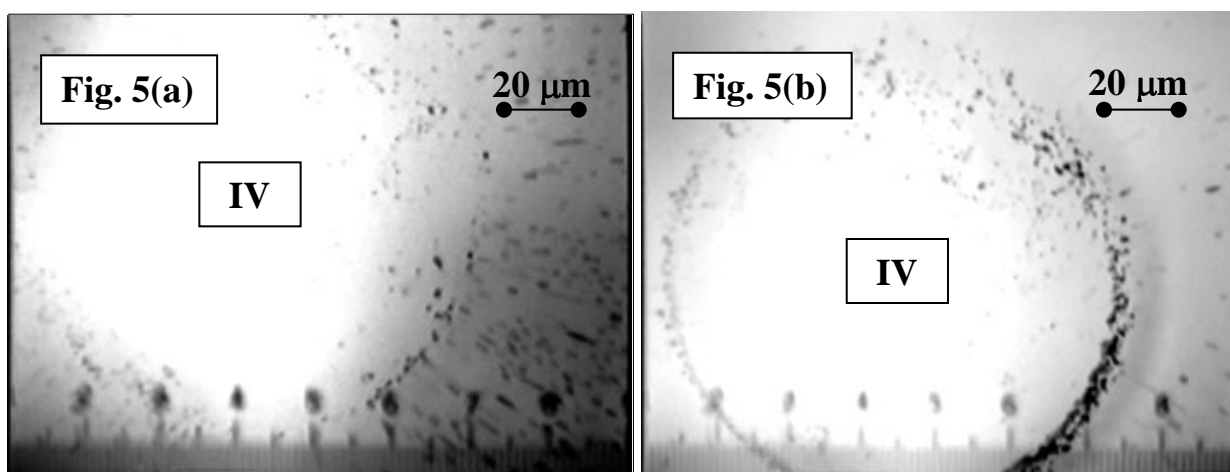


Figure 5 These photographs represent two snapshots in the lifetime of a drop of pure chloroform evaporating in ambient air. Silica beads of 2 μm diameter (dark particles) were used to track the convective flow by video microscopy. The total lifetime of the droplet was 37 s. Fig. 5(a) depicts $t = 30$ s and Fig. 5(b) depicts $t = 33$ s. Together these two frames depict the progressive accumulation of solute at the boundary of the stationary cap (region IV) caused by the Bénard convection in region III. As time proceeds, the solute in regions II and III migrates toward the edge of the stagnant cap forming the black ring shown on the right.

CONCLUSION

Liquid ribbons of solutions of copper hexanoate in a volatile solvent like chloroform or isopropanol were drawn on a glass slide using fine capillaries. After solvent evaporation, the solute was observed to segregate into multiple pairs of stripes much narrower than the initial

ribbon diameter. These stripes are then converted to pure copper by annealing. The viscosity and volume per length deposited (which depends on the shape and size of the dispensing tool) strongly influence the thickness, width and number of lines formed during the drying process. Previous studies have shown that contact line pinning due to surface roughness or chemical inhomogeneities cause solute accretion at the three phase contact line. Besides this mechanism of solute accretion, we have identified the formation of Bénard-Marangoni convection patterns which assist solute accretion in the liquid interior. For highly volatile solvents as those used in this study, surface convective flows closer to the contact line help guide and migrate solute toward the periphery of a stagnant region centered about the apex of the drying liquid structure. Further control and optimization of this process can help enlist this phenomenon of self-organized line narrowing for the direct printing of fine metallic lines from a wider liquid precursor [12].

ACKNOWLEDGEMENTS

The authors would like to thank Anton Darhuber and Scott Miller for assistance.

REFERENCES

1. R.D. Deegan, O. Bakajin, T.F. Dupont, G. Huber, S.R. Nagel and T.A. Witten, *Nature* **389**, 827 (1997).
2. R.D. Deegan, *Phys. Rev. E* **61**, 475 (2000).
3. J. Conway, H. Korns, and M. R. Fisch, *Langmuir* **13**, 426 (1997).
4. S. Maenosono, C. D. Dushkin, S. Saita, and Y. Yamaguchi, *Langmuir* **15**, 957 (1999).
5. E. Adachi, A. S. Dimitrov, and K. Nagayama, *Langmuir* **11**, 1057 (1995).
6. P. G. deGennes, *Rev. Mod. Phys.* **57**, 827 (1985).
7. J.F. Joanny and P.G. deGennes, *J. Chem. Phys.* **81**, 552 (1984).
8. C.M. Hong, H. Gleskova and S. Wagner, *Mat. Res. Soc. Symp. Proc.* **471**, 35 (1997).
9. N. Zhang and W. Yang, *J. Heat Transfer* **104**, 656 (1982).
10. N. Zhang and W. Yang, *J. of Heat Transfer* **105**, 908 (1983).
11. J. C. Duh and W. Yang, *Numerical Heat Transfer, Part A* **16**, 129 (1989).
12. T. Cuk, S. M. Troian, C. M. Hong and S. Wagner, *Appl. Phys. Lett.*, to be published.